JSAE 20190XXX
SAE 2019-YY-YYYY

Modelling Pressure Losses in Gasoline Particulate Filters in High Flow Regimes and Temperatures

M. Prantoni, S. Aleksandrova, H. Medina, J. Saul, S. Benjamin
Coventry University

O. Garcia Afonso
Jaguar Land Rover

ABSTRACT

This study presents a one-dimensional model for the prediction of the pressure loss across a wall-flow gasoline particulate filter (GPF). The model is an extension of the earlier models of Bissett [1] and Kostandopoulos and Johnson [2] to the turbulent flow regime, which may occur at high flow rates and temperatures characteristic of gasoline engine exhaust. A strength of the proposed model is that only one parameter (wall permeability) needs to be calibrated. An experimental study of flow losses for cold and hot flow is presented, and a good agreement is demonstrated. Unlike zero-dimensional models, this model provides information about the flow along the channels and thus can be extended for studies of soot and ash accumulation, heat transfer and reaction kinetics.

INTRODUCTION

Following the introduction of new regulations limiting the Particulate Matter (PM) emissions from gasoline engines, many automotive companies have introduced Gasoline Particulate Filters in their vehicles. Although the GPFs are overall the most effective way of reducing the PM emissions, they affect the performance of the engine in terms of fuel efficiency. Integration of the wall-flow filter in the exhaust system produces a high backpressure, and the engine must provide extra work to overcome it. Therefore, the knowledge and the ability to accurately predict the backpressure caused by the monolith has become more important for automotive companies in optimization of their vehicles.

Over the years many zero-dimensional (i.e. [2, 3, 4, 5, 6]), one-dimensional (i.e. [2, 5, 7, 8, 9]) and two-dimensional (i.e. [10, 11]) models predicting the pressure drop of a wall-flow monolith have been proposed. To date, zero-dimensional and one-dimensional models have received more attention than to two-dimensional models, as the latter are far more complex and provide relatively little or no advantages compared to the former ones [13]. Zero-dimensional models are the most desirable as they provide quick solutions and are easy to implement. However, they generally have lower accuracy, as they are often generated as approximations of one-dimensional models' solutions through the uncoupling of the pressure drop contributions of different sources. One-dimensional models have fewer approximations of the flow physics with respect to zero-dimensional models and therefore they are more likely to perform well over a wider range of parameters. They also provide information about flow distribution inside the channels, which is important for soot and ash accumulation analysis. Depending on the formulation they may require numerical solutions (i.e. [1, 7, 8, 9]), which are more time consuming and slow down the optimization process. A review of most of these models can be found in [12, 13, 14].

With a few exceptions, these models have been developed for the predictions of Diesel Particulate Filters (DPFs) backpressure and have shown a certain degree of success for DPFs operating conditions. However, because of the different operating conditions in GPFs, such as higher flow rates and temperatures, different geometry and wall properties of the filters, these models may not be suitable for predicting the GPFs backpressure in the full operating range. Most recent studies of GPFs (i.e. [15, 16]) focus more on soot/ash loading and PM transport modelling, assuming that the clean filter pressure losses are well understood. This is not the case for the turbulent flow regime, thus, there is a need to develop a new predictive model which is capable of predicting the pressure drop under these conditions.

This work presents a one-dimensional model based on the work of Bissett [1] and Kostandopoulos and Johnson [2]. The modelling results are compared to experimental measurement of pressure losses of four different filter cores in cold and hot flow conditions. By taking into account the turbulent flow losses and

incorporating a density correction based on the channels' pressure, the model is a step towards building a complete physics based model for predicting pressure loss in wall-flow filters over a wide range of parameters.

EXISTING LAMINAR FLOW MODEL

The first significant one-dimensional particulate filter study was presented by Bissett [1] in 1984. Although the aim of the model was primarily to gain a deeper understanding of the regeneration process in wall-flow Diesel Particulate Filters, its formulation laid the foundations for the development of predictive models more focused on the pressure drop characteristics of the filters.

A few years later Kostandopoulos and Johnson [2] proposed a simple one-dimensional flow model (here referred as Bissett-Konstandopoulos model as this model is a subset of equations of Bissett's model) and assessed it against the available experimental pressure drop data of typical wall-flow monoliths with the intent of providing a tool for the rational engineering design and optimization of DPFs. The principal assumptions on which the model is based are:

- the monolith is radially insulated, so that all inlet cells and all outlet cells can be described by the behavior of a single representative, inlet or outlet, cell;
- the flow is in steady state;
- the flow within the channels is laminar;
- the temperatures of the flow entering and leaving the filter are approximately equal (isothermal flow);
- the gas properties are spatially and temporally uniform.

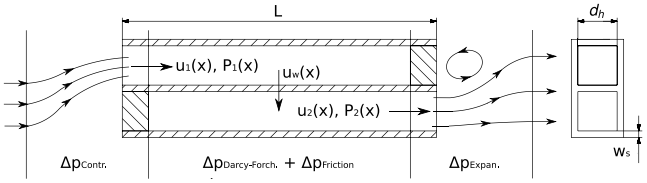

Figure 1. Monolith flow model schematic.

Additional assumptions, directly or indirectly reported are:

- the flow distribution at the entrance of the monolith is uniform;
- the flow profile in the channels is unaffected by the suction/injection from the porous wall and it is fully developed;
- the slip effects are neglected;
- there is no axial momentum transfer at the porous wall surface;
- the Forchheimer losses are negligible.

Under these assumptions, the complex behavior of the flow within the particulate filter can be described by a one-dimensional fluid dynamics model, comprising four differential equations, describing the mass and momentum balance in the inlet and outlet channels, and an algebraic one, describing the wall pressure drop:

$$\frac{d}{dx}(\rho u_1) = -\frac{4}{d_h}\rho u_w, \quad (1)$$

$$\frac{d}{dx}(\rho u_2) = +\frac{4}{d_h}\rho u_w, \quad (2)$$

$$\frac{d}{dx}(\rho u_1^2) = -\frac{d}{dx}(P_1) - \frac{2}{d_h}C_{f,1}\rho u_1^2, \quad (3)$$

$$\frac{d}{dx}(\rho u_2^2) = -\frac{d}{dx}(P_2) - \frac{2}{d_h}C_{f,2}\rho u_2^2, \quad (4)$$

$$P_1 - P_2 = \frac{\mu}{k}u_w w_s, \quad (5)$$

where:

- $u_1(x)$ and $u_2(x)$ are the local mean cross-sectional axial velocities along the inlet and outlet channels and u_w is the local mean velocity in the porous wall,
- $P_1(x)$ and $P_2(x)$ are the local mean cross-sectional pressures along the inlet and outlet channels,
- $C_{f,1}(x)$ and $C_{f,2}(x)$ are the local Fanning friction factors along the inlet and outlet channels,
- d_h is the cell hydraulic diameter,
- w_s is the porous wall thickness,
- ρ is the gas density,
- μ is the gas dynamic viscosity,
- k is the filter permeability,
- x is the axial coordinate, varying from 0 at the entrance of the filter to L at the exit of the filter.

The model formulation is then completed through the following boundary conditions:

$$u_1(0) = U, \quad (6)$$

$$u_2(0) = 0, \quad (7)$$

$$P_2(L) = P_{Atm.}, \quad (8)$$

where:

- U is the mean flow velocity at the entrance of the inlet channel (at $x = 0$),
- $P_{Atm.}$ is the atmospheric pressure (which can be replaced with pressure at the outlet of the filter).

Eq. (6) states that at the entrance of the inlet cell the velocity is known, Eq. (7) states that at the entrance of the outlet cell the velocity is zero, as the plug is impermeable, while Eq. (8) states that the pressure at the exit of the outlet cell is known (and equal to the atmospheric pressure in this case).

Because the flow is assumed to be laminar, the Fanning friction factor, for a duct of square cross section, can be defined as:

$$C_{f,i} = \frac{14.227}{Re_i} \quad \text{or} \quad C_{f,i}Re_i = 14.227, \quad (9)$$

where $Re_i = \frac{\rho d_h u_i}{\mu}$ $(i = 1, 2)$ is the local Reynolds number along the channel.

As the product of the local friction factor and the local Reynolds number is a constant, this assumption simplifies the model considerably, so that it can be solved analytically. The total pressure drop of the filter is then given by:

$$\Delta P_{Konst.} = \left\{ A_1 + A_2 \left[\frac{1}{2} + \frac{c_1}{g_1}(e^{g_1} - 1) + \frac{c_2}{g_2}(e^{g_2} - 1) \right] + c_1 g_1 + c_2 g_2 \right\} \frac{\mu U d_h w_s}{4Lk}, \quad (10)$$

with:

$$A_1 = \frac{k}{d_h w_s} \frac{4L}{d_h} Re, \quad (11)$$

$$A_2 = 8 C_f Re \frac{k}{d_h w_s} \left(\frac{L}{d_h} \right)^2, \quad (12)$$

$$g_1 = A_1 - \sqrt{A_1^2 + 2A_2}, \quad (13)$$

$$g_2 = A_1 + \sqrt{A_1^2 + 2A_2}, \quad (14)$$

$$c_1 = -\frac{1}{2} - c_2, \quad (15)$$

$$c_2 = \frac{1}{2} \left(\frac{e^{g_1} + 1}{e^{g_2} - e^{g_1}} \right). \quad (16)$$

As stated by Kostandopoulos and Johnson [2], this was the "first comprehensive relation that expresses explicitly the pressure drop of clean wall-flow monoliths in terms of their manufacturing parameters and exhaust properties," and it was a breakthrough towards the advancement of understanding the flow physics within the particulate filters and a useful tool for their design optimization.

However, in order to correctly utilize this model, its limitations need to be understood properly. In particular, the implementation of Eq. (9) is only valid for laminar flow, as outside this range the product of the friction factor and the Reynolds number is not a constant, and their product increases considerably with increasing Reynolds number. Therefore, the physical validity of Bissett-Kostandopoulos [2] formulation is restricted to laminar flow only. Additionally, this model does not account for the density variation of the exhaust gas along the channels, which may become important especially at high values of the backpressure, and the losses due to contraction and expansion at the inlet and outlet of the filter, which may become important at high velocities. Although attempts to include the density variation along the channels into the model have been made [4], these are mostly based on zero-dimensional model and thus the information about the flow inside the channels is lost. Moreover, the zero-dimensional model of [2] is itself based on extra assumptions and thus is less accurate than the original one-dimensional model.

Because of higher flow rates and temperatures, different geometry and wall properties of the filters the flow within GPFs is likely to be turbulent for some of the engine operational conditions.

For example, the exhaust mass flow rate for a 4L naturally aspired gasoline engine can exceed $1000\ [kg/h]$. For a 300-12 uncoated filter with a typical diameter of $D = 120\ [mm]$ this would correspond to a Reynolds number at the entrance of the inlet channel of above 2000 at $T = 700\ [℃]$. The Reynolds number will become even higher for coated filters, soot-loaded filters, filters with thicker wall and/or lower cell density, at lower temperature (i.e. during cold start), for larger engines or turbocharged and supercharged applications.

Although high local Reynolds numbers do not necessarily mean that transition to turbulent regime is present, the experiments conducted in this study, as presented later, show that there is evidence of turbulent flow.

As reported by Masoudi [17], turbulent flow regimes within the filter channels can be present even in DPFs. Moreover, due to the higher pressure drop and channel flow velocity the density variation and the contraction and expansion losses may play an important role.

The Bissett-Kostandopoulos [2] model was not designed for these flow conditions (turbulent flow, high temperature, high pressure drop, high channel flow velocity). The model proposed here aims to fill these gaps.

DEVELOPMENT OF THE MODEL

The proposed model is based on the same equations (Eqs. (1) - (5)) and the same assumptions as Bissett-Kostandopoulos [2] model, with the exception of the laminar flow assumption and the definition of the gas density. The irreversible pressure losses due to contraction and expansion are added to the total pressure loss to complete the model. Here, pressure loss contributions from different sources are discussed in detail.

COUPLED FRICTION AND THROUGH WALL LOSSES

Under the assumption of fully developed flow, the friction factor for a channel of circular cross section can be calculated through the Colebrook equation [18] for the full spectrum of flow regimes. However, the Colebrook equation is an implicit equation with no closed solution. Many approximate solutions of the equation exists (see review by Brkić [19]), including Churchill's correlation [20], which presents the advantage of covering the flow regimes from laminar to turbulent in a simple and explicit formula:

$$C_{f,i} = 2 \left(\left(\frac{8}{Re_i} \right)^{12} + \frac{1}{\left[2.457 \ln \left(\frac{1}{\left(\frac{7}{Re_i} \right)^{0.9} + 0.27\varepsilon} \right) \right]^{16} + \left(\frac{37530}{Re_i} \right)^{16}} \right)^{\frac{1}{12}}, \quad (17)$$

where:

- $Re_i = \frac{\rho d_h u_i}{\mu}$ $(i = 1,2)$ is the local Reynolds number along the channel,
- ε is the surface roughness.

Thus, in order to account for turbulent flow losses, Churchill's correlation (Eq. (17)) is implemented for the friction factor. As a result, the model uses the appropriate friction factor (whether laminar or turbulent) based on the local Reynolds number value. Note that strictly speaking Eq. (17) is only valid for fully developed flow in channels with non-porous walls.

Since, Eq. (17) has been derived for channels of circular cross section, a correction factor is required to account for the square cross-section used here. Jones [21] investigated the friction factor in ducts with different cross sections and proposed a simple empirical correction factor, derived from experimental data, based on a modified Reynolds number to correlate the friction factor of circular cross section ducts to other shapes. According to Jones [21], the correlation between circular cross section and square cross section is:

$$Re_{Square,i} = \frac{16}{14.227} Re_{Circular,i} = \frac{16}{14.227} \frac{\rho d_h u_i}{\mu}, \quad (18)$$

where:

- $Re_{Circular,i}$ is the local Reynolds number for ducts of circular cross-section,
- $Re_{Square,i}$ is the local Reynolds number for ducts of square cross-section.

Thus, using $Re_{Square,i}$ instead of Re_i in Eq. (17) gives an expression for the friction factor in ducts of square cross section.

Substituting, Eq. (17) and Eq. (18) into Eq. (3) and Eq. (4) and following the same procedure as Kostandopoulos and Johnson [2], to reduce the system of equations (Eqs. (1) - (5)) to a single one, leads to the following second order non-linear differential equation:

$$\frac{\mu}{k} w_s \frac{d_h}{4} \frac{d^2}{dx^2}(u_2) - 2\rho U \frac{d}{dx}(u_2) + \frac{2}{d_h} C_{f,1} \rho (U^2 + u_2^2 - 2u_2 U) - \frac{2}{d_h} C_{f,2} \rho (U^2 + u_2^2 - 2u_2 U) = 0 . \quad (19)$$

Eq. (19) can be solved numerically for u_2 with the following boundary conditions:

$$u_2(0) = 0, \quad (20)$$
$$u_2(L) = U. \quad (21)$$

Once u_2 is known, the other variables can be easily found numerically from the system of equations (Eqs. (1) - (5)). In order, u_w is calculated from Eq. (2), u_1 is calculated from Eq. (1), P_2 is calculated from Eq. (4) with Eq. (8) as boundary condition and finally P_1 is calculated from Eq. (5).

Once P_1 and P_2 are known, the filter pressure drop due to coupled friction and through wall losses can be calculated as:

$$\Delta P_{Friction+ThroughWall} = P_1(0) - P_2(L). \quad (22)$$

Similar to the original laminar flow solution presented by Kostandopoulos and Johnson [2], the through wall losses and the losses due to friction are coupled. This means, for example, that changing some filter parameters (i.e. the permeability, the channels hydraulic diameter, others) would affect simultaneously the trend of the velocity within the channels, and consequently the losses due to friction, and the trend of the velocity within the porous wall, and consequently the through wall losses. Decoupling of these losses in the laminar flow model presented in [2] may lead to considerable errors for some parameter ranges.

CONTRACTION AND EXPANSION LOSSES

The flow passing through the contraction and expansion at the entrance and exit of the filter produces extra losses, called contraction and expansion losses. These irreversible losses are usually expressed in terms of the dynamic pressure:

$$\Delta P_{Contr.} = \zeta_{Contr.} \frac{\rho U^2}{2}, \quad (23)$$
$$\Delta P_{Exp.} = \zeta_{Exp.} \frac{\rho U^2}{2}, \quad (24)$$

where:

- $\zeta_{Contr.}$ is the contraction loss coefficient,
- $\zeta_{Exp.}$ is the expansion loss coefficient,
- U is the mean cross section velocity in the smaller duct (or channel).

Due to the relevance of the contraction and expansion losses in hydraulic applications, they have been extensively investigated over the years, both theoretically and experimentally. A review of some of these studies can be found in [22]. Generally, the contraction and expansion loss coefficients depend on the geometry (contraction area ratio, abrupt or continuous change, single opening or multiple openings), and the flow properties (laminar/turbulent flow regime and Reynolds number). Despite the wide number of investigations, a unique definition of these coefficients has not been achieved.

The most widespread and accepted theoretical formula for the expansion loss coefficient is obtained from the Borda-Carnot equation [23]:

$$\zeta_{Exp.} = \left(1 - \frac{A_1}{A_2}\right)^2, \quad (25)$$

where A_1 and A_2 are the areas of the smaller and larger cross-section, respectively. Figure 2 shows how the expansion loss coefficient varies with the expansion area ratio.

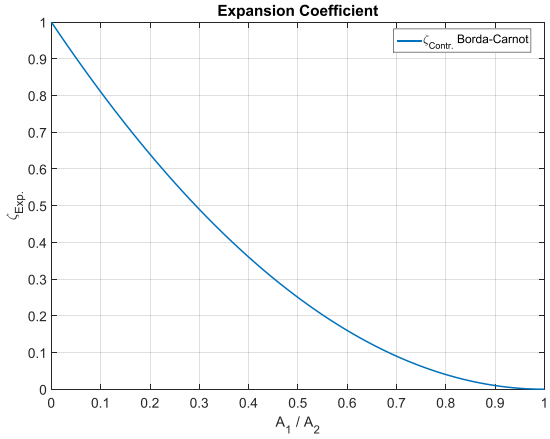

Figure 2. Expansion coefficient.

For the contraction loss coefficient, however, various definitions that can be found in the literature are purely empirical and based on experimental data. The correlations proposed by Sullivan [24], Merriman [25], Weisbach [26] and Kays [27] (for which the fitting has been performed by Haralampous [5]) are:

$$\zeta_{Contr.} = 0.5\left(1 - \frac{A_1}{A_2}\right), \tag{26}$$

$$\zeta_{Contr.} = \left(\frac{1}{c} - 1\right)^2, \qquad c = 0.582 + \frac{0.0418}{1.1 - \sqrt{\frac{A_1}{A_2}}}, \tag{27}$$

$$\zeta_{Contr.} = 0.63 + 0.37\left(\frac{A_1}{A_2}\right)^3, \tag{28}$$

$$\zeta_{Contr.,Laminar} = 1.1 - 0.4\frac{A_1}{A_2}, \tag{29}$$

Figure 3 shows how the contraction loss coefficient, calculated with these formulae, varies with the contraction area ratio.

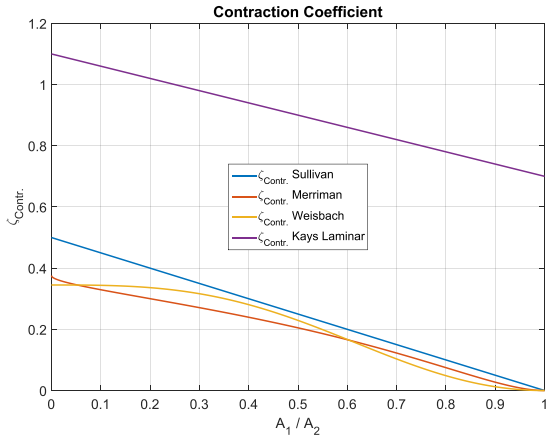

Figure 3. Contraction coefficient.

Eqs. (26) - (28) have been shown to agree reasonably well with experiments for the turbulent flow regime [22]. With laminar flow there are fewer studies and the uncertainties are higher. In fact, Eq. (29) does not seem to be well validated against the experimental data of Kays [27] for low Reynolds numbers, in multiple channel geometries.

Although these expressions are mostly validated for sudden contraction and expansion in a single channel, in absence of more reliable data for the particular geometry of wall-flow filters, they can be used as good approximations [3].

In the model presented here, the contraction and expansion losses, defined respectively by Eq. (30) and Eq. (31), are added in series to the pressure drop resulting from the solution of the model.

$$\Delta P_{Contr.} = \zeta_{Contr.}\frac{\rho_{Inlet}U^2}{2}, \tag{30}$$

$$\Delta P_{Exp.} = \zeta_{Exp.}\frac{\rho_{Outlet}U^2}{2}, \tag{31}$$

where the contraction and expansion loss coefficients are defined by Eq. (26) and Eq. (25) and ρ_{Inlet} and ρ_{Outlet}, the densities at the inlet and outlet, are discussed in the next section.

Note that in some models, such as [4, 17], the contraction and expansion loss coefficients are estimated by fitting experimental data. This introduces an extra calibration parameter into the model and may result in unrealistic values of the coefficients, as evident in [4].

DENSITY VARIATION EFFECTS

With the increase of the total pressure drop and of the absolute local pressure within the channels the effect of the density variation may become non-negligible and it should be accounted for [4]. Thus, an accurate formulation of the model would require using the local gas density value corresponding to the actual local pressure. According to the ideal gas law, the density is defined as:

$$\rho = \frac{M}{RT}P, \tag{32}$$

where M is the molar mass of the gas, P its local pressure, T its local temperature and R is the universal gas constant.

Although it is possible to account for the density changes along the inlet and outlet channel in a one-dimensional model [9, 14], this requires numerical solution of a system of ordinary differential equations. Simplifications are possible but involve additional assumptions about density or velocity distribution [14].

In the proposed formulation, in order to simplify the solution, the density of the gas has been assumed to be spatially constant. The effect of the density variation due to the backpressure can be still accounted for through a reasonable approximation, commonly adopted in many engineering fluid dynamics problems, by defining the density of the gas as the mean density value based on the average local pressure between the inlet and outlet channel [4]. Thus, the density is defined as:

$$\rho = \frac{M}{RT}\frac{1}{L}\int_0^L \frac{(P_1 + P_2)}{2}\,dx, \tag{33}$$

where P_1 is the local pressure along the inlet channel and P_2 is the local pressure along the outlet channel.

Introducing this new definition of the density requires knowledge of the pressure distribution inside the channels and thus the proposed model requires an iterative solution, which is summarized in the next section.

SUMMARY

The proposed predictive one-dimensional model takes into account the coupled effect of the friction (including turbulent regime) and through wall losses, the effect of the density change and the losses due to contraction and expansion.

The pressure drop due to friction and through wall losses is given by Eq. (22), as described earlier, while the losses due to contraction and expansion are given by Eq. (30) and Eq. (31). The effect of the density change is accounted for through an iterative process, as the local pressure in the inlet and outlet channels used in Eq. (33) are not known a priori.

Thus, the iterative solution process consists of the following steps:

1) At the first iteration step, Eq. (22) is solved using a density based on the outlet pressure $\rho_{it=1} = \frac{M}{RT} P_2(L)$.
2) The contraction and expansion losses, as defined in Eq. (30) and Eq. (31), are added to Eq. (22). As after the first step the local pressure in the inlet and outlet channel are known, the inlet and outlet density used in Eq. (30) and Eq. (31) can be defined as $\rho_{Inlet,it=1} = \frac{M}{RT} P_1(0)$ and $\rho_{Outlet,it=1} = \frac{M}{RT} P_2(L)$, respectively.
3) The mean density within the channels is recalculated using Eq. (33) and it used as input density for the successive iteration.
4) Steps 1) to 3) are repeated n times, until $\left|\frac{\Delta P_{it=n-1} - \Delta P_{it=n}}{\Delta P_{it=n-1}}\right| \times 100 < 0.005$, which is the criterion selected for the convergence here.

EXPERIMENTS

A series of experiments have been performed to measure pressure losses for 4 different filter cores. These are presented in full in a different paper (currently under review), however a subset of the data is presented here along with a brief description of the experimental data in order to validate the model.

EXPERIMENTAL RIG AND PROCEDURE

The hot flow rig is shown in Figure 4. Compressed air supplies the two 36 $[kW]$ heaters (1). A double-skin nozzle (2) was designed to mix the hot air from the heaters and provide a uniform flow distribution. An upstream instrumentation section (3) contains 4 pressure tappings located 30 $[mm]$ upstream of the core spaced equally around the circumference of the pipe, and a thermocouple located 25 $[mm]$ upstream of the core. The test section (4) holds the core and contains three K-type thermocouples touching the core surface. A downstream instrumentation section (5) contains 4 pressure tappings located 95 $[mm]$ downstream of the core and spaced equally around the circumference of the pipe. Another thermocouple is located 75 $[mm]$ downstream of the test section. An outlet sleeve with an adjustable duct attached (6) directs the hot air into the extractor duct.

Table 1. Core sample properties

Property	Unit	Core #1	Core #2	Core #3	Core #4
Cell density	$[Cpsi]$	300	300	300	300
Wall thickness	$[mil]$	8	8	8	12
Length	$[mm]$	125	125	100	125
Filter effective diameter	$[mm]$	50	50	50	50
Coated	$[-]$	No	Yes	Yes	Yes
Cell hydraulic diameter	$[mm]$	1.26	1.22	1.22	1.13
Wall thickness	$[mm]$	0.203	0.238	0.238	0.327
Median pore size	$[\mu m]$	17.5	10.3	10.3	12.3
Median porosity	$[-]$	0.64	0.59	0.59	0.55

Pressure measurements upstream and downstream of the test section were performed using digital manometers with accuracy within $\pm 0.25\%$ of the reading. A calibrated Viscous Flow Meter (VFM) was used to set the mass flow rate. Temperatures were measured using K-type thermocouples with an accuracy of ± 2.5 [℃].

For each temperature point, around 2 hours were needed to reach thermal equilibrium (which was assumed when the core surface temperature change was within 2 [℃] over a period of 5 minutes). Good repeatability of the results was confirmed regardless of whether the temperature was increased from the previous test point or decreased.

CORE SAMPLES

The testing was performed with 58 $[mm]$ diameter cordierite filter core samples. Four samples were used as specified in Table 1. Core #1 is uncoated, while cores #2, #3 and #4 have a catalyst coating applied. The monolith channel wall thickness and hydraulic diameter were estimated using the data provided by the manufacturer. The core samples were enclosed in steel sample holders, with a circular opening of 50 $[mm]$ diameter available to the flow at both ends.

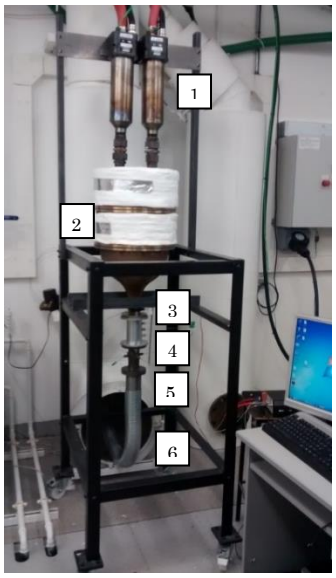

Figure 4. Rig

EXPERIMENTAL EVIDENCE OF FLOW REGIME CHANGE

The cold flow test results are shown in Figure 5, while a selection of tests at different temperatures are shown in Figure 7 and Figure 8. As expected, the pressure loss is lowest for the uncoated filter core #1, and highest for the filter core #4 with the thickest coated walls. Cores #2 and #3 have the same nominal geometrical and coating parameters and only differ in length. The measured pressure drop is lower for the longer core #2, which is in agreement with some other studies of the effect of filter length on the pressure drop [6] and is discussed further in the modelling section.

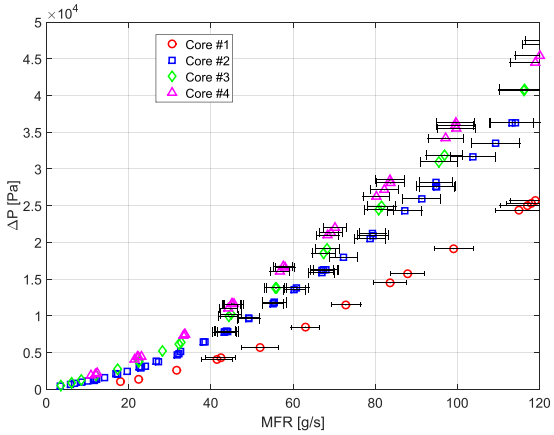

Figure 5. Pressure loss versus mass flow rate (cold flow at 20 [°C])

Figure 6 shows change of the non-dimensional pressure,

$$\Delta P^* = \frac{\Delta P}{\frac{1}{2}\rho U^2},$$

with the Reynolds number at the entrance of the inlet channel,

$$Re = \frac{\rho U d_h}{\mu}.$$

Here, the velocity at the entrance of the inlet channel is defined as

$$U = \frac{MFR}{\rho\, OFA},$$

with MFR being the experimental mass flow rate, OFA the filter open frontal area, d_h the channel hydraulic diameter, while ρ and μ are the density and dynamic viscosity of the air upstream the core.

It can be seen from Figure 6 that all cores show similar trends, although it is clear that other non-dimensional groups (which will depend on the filter properties such as permeability, length, etc.) play an important role. There is a change in the trend between lower and higher values of the Reynolds number. Two trend lines are added on top of the experimental data showing the characteristic slope for laminar (Re^{-1}) and turbulent ($Re^{-1/4}$ according to Blasius formula [23]) friction loss. The factors for these (C_1 and C_2 in the legend) are chosen arbitrarily so that the slope lines are shown next to the test data. The data follow the laminar trend up to $Re < 1800$ and the turbulent trend for $Re > 3000$. This is also in agreement with the study of Jones [21], where it is reported that the laminar regime ends earlier in ducts with square cross-section with respect to ducts with circular cross-section. If the friction losses remained laminar (i.e. proportional to velocity), then the inertial losses would dominate at high mass flow rates with the non-dimensional pressure becoming nearly constant. Thus, the experimental results demonstrate a clear change of the pressure loss trend consistent with the transition from the laminar to turbulent regime.

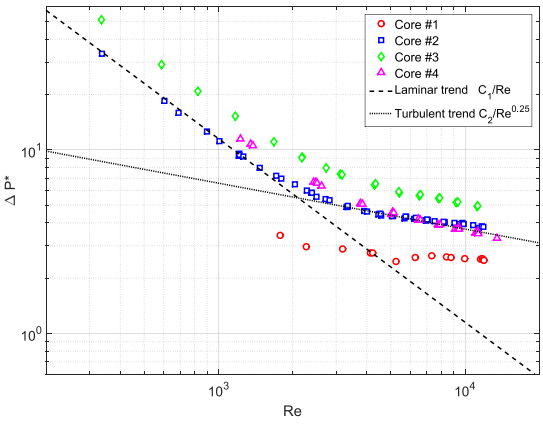

Figure 6. Non-dimensional pressure loss versus Reynolds number at the entrance of the inlet channel (cold flow at 20 [°C])

ASSESSMENT OF THE MODEL

In this section the proposed model is assessed against experimental data and compared with the Bissett-Konstandopoulos [2] model (with added contraction and expansion losses).

Before the assessment, the permeability calibration, required for calculation of through wall losses, is presented.

PERMEABILITY CALIBRATION

One of the main advantages of the model is the fact that only one parameter needs to be calibrated through experimental testing, namely the porous wall permeability.

Two different methods could be used to estimate the permeability. One method would involve finding a permeability value by using linear regression analysis to fit the whole model to the experimental data. However, it is time-consuming and an inefficient process. Since at ambient temperature and low mass flow rate (laminar regime) the model is nearly identical to the Bissett-Kostandopoulos [2] model, the second method involves using their explicit expression to find the permeability value that results in fittings the experimental data in the laminar flow regime. Under these flow conditions, the density changes along the channels due to backpressure are negligible and the resulting permeability value is a good approximation. Note that it is preferable to only use the experimental data in the laminar regime at ambient temperature for the calibration. In this range, pressure losses are well understood and contribution of through wall losses is higher compared to inertial losses, thus better accuracy can be achieved.

For the Bissett-Kostandopoulos [2] model, the pressure drop is expressed by Eqs. (10), (23) and (24), and thus the permeability can be estimated using the least square fit. The resulting values of the permeability for cores #1, #2, #3 and #4 are $k = 5.5 \times 10^{-12}\ [m^2]$, $k = 1.9 \times 10^{-13}\ [m^2]$, $k = 1.4 \times 10^{-13}\ [m^2]$ and $k = 1.7 \times 10^{-13}\ [m^2]$, respectively. Comparing the permeability estimated through this method for core #1 with the one reported in [28], which was derived experimentally through wafer samples testing of the same core, shows a good agreement. This further confirms the validity of the method used here. The permeability values reported above were used in the final model validation.

MODEL VALIDATION AND COMPARISON WITH THE BISSETT-KONSTANDOPOULOS MODEL

The proposed model has been implemented in Matlab. The ordinary differential equations (Eq. (19), with boundary conditions Eq. (20) and (21), and Eq. (4), with boundary condition Eq. (8)) have been solved with the boundary value problems solver bvp5c. bvp5c is a finite difference code that uses the four-stage Lobatto IIIa formula, which is implemented as an implicit Runge-Kutta formula. The script takes between 1 to 20 seconds to converge for each single pressure drop prediction, depending on the flow conditions. Any other one-dimensional boundary value problem solver can be used.

The present model extends the Bissett-Kostandopoulos [2] model to account for the turbulent friction losses and change in density. Thus, two comparison have been made to evaluate separately the effect of each contribution.

Figure 7 shows a comparison between the proposed model with the experimental results and the Bissett-Kostandopoulos [2] model for all cores and flow conditions, while in Figure 8 the density "correction" has been added to the Bissett-Kostandopoulos [2] model. For the Bissett-Kostandopoulos [2] model the predictions within the laminar flow regime have been plotted with dotted lines, to indicate the limit up to which the model can be used (as outside its assumptions are not valid).

Note that the original one-dimensional Bissett-Kostandopoulos [2] model does not include the contraction and expansion losses. Therefore, here the losses described by Eq. (30) - (31) have been added to the Bissett-Kostandopoulos [2] model, in both cases.

Comparing the Bissett-Kostandopoulos [2] model (Figure 7) with the corresponding density "corrected" version (Figure 8) allows the effect of the density change to be evaluated. Within the laminar flow regime and at low temperatures, when the pressure drop is small with respect to the filter outlet pressure (atmospheric pressure in this case), the effect of the density change is negligible. However, with increasing temperature, and hence backpressure, this effect becomes increasingly significant. In the coated filters and at $T = 680$ [℃], the inclusion of the change in density may reduce the deviation between measurements and predictions from up to $30 - 40\%$ to about 10% .

From Figure 8, then, it can clearly be seen that the Bissett-Kostandopoulos [2] model deviates from the experimental trend immediately outside the laminar flow regime (for which it was designed), and cannot be used for high Reynolds numbers characteristic of the turbulent flow regime. It can be seen that the inclusion of the turbulent friction factor effectively extends the Bissett-Kostandopoulos [2] model to the turbulent flow regime. Figure 7 and Figure 8 show that by including the generalized friction factor (Eq. (17)) and the density variation (Eq. (33)) good predictions of pressure loss for all Reynolds numbers can be made.

For all cores, the difference between the model predictions and experimental measurements is within $\pm 10\%$, with exception of a few data points. This means that a great part of the predictions lay within the experimental uncertainty.

Note that the maximum mass flow rate considered here is $120\ [g/s]$ for a filter core with diameter $50\ [mm]$. This is equivalent to $690\ [g/s]$ (or $2500\ [kg/h]$) for a filter with diameter $120\ [mm]$, which is a common size for GPFs. Although this mass flow rate is much higher than the mean mass flow rate in most of the engines operating conditions, it can occur in some applications as discussed earlier. The model can be further developed to account for transients effects, in which case it can be adopted for pulsating flows where the instantaneous mass flow can be twice as high as the mean. Additionally, considering high mass flow rates ensures that the model's prediction of the flow physics is valid whatever the conditions.

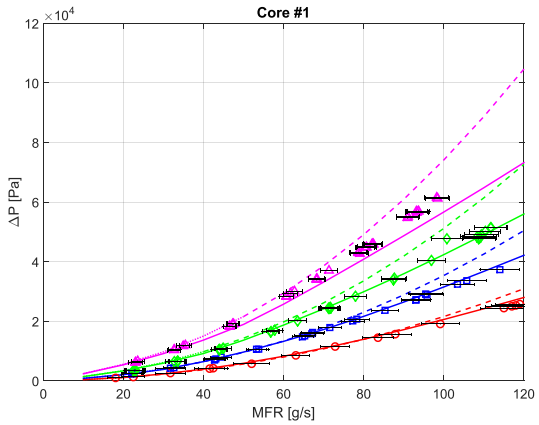

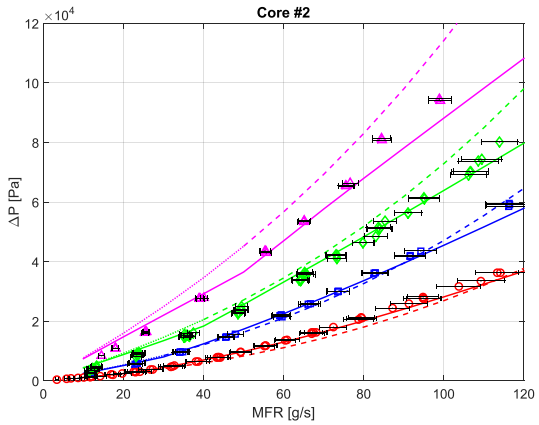

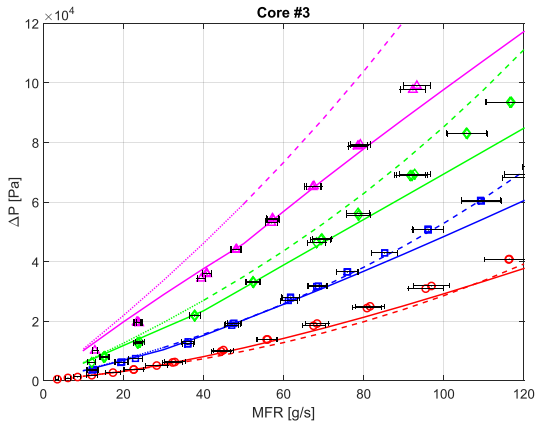

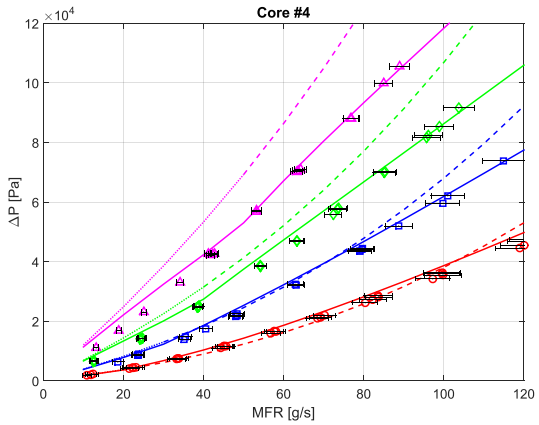

Figure 7. Comparison of the proposed model with experiments and Bissett-Konstandopoulos [2] model with contraction and expansion losses. Dotted part of the lines indicates laminar regime.

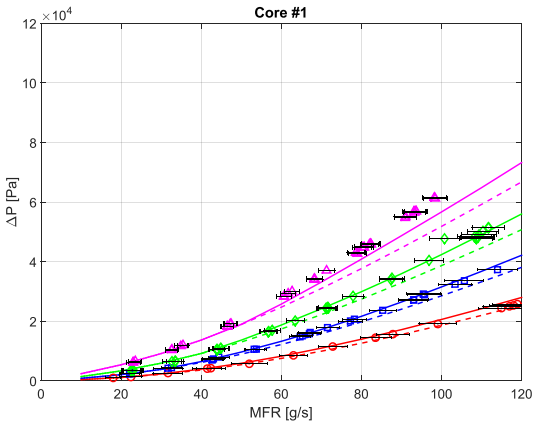

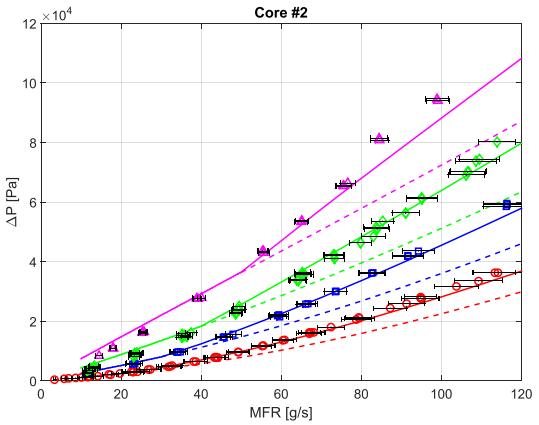

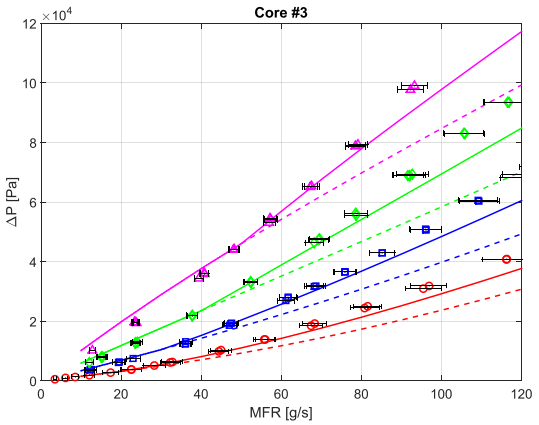

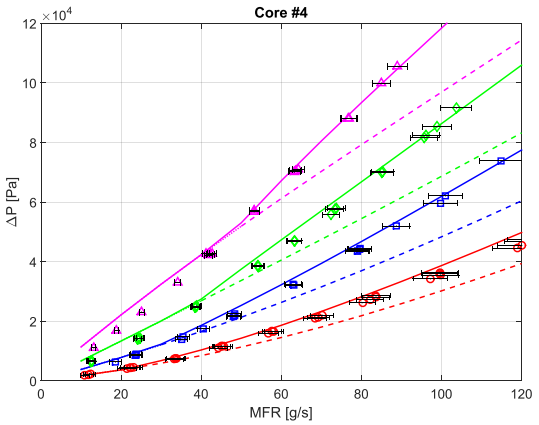

Figure 8. Comparison of the proposed model with experiments and Bissett-Konstandopoulos [2] model with contraction and expansion losses and density change effects. Dotted part of the lines indicates laminar regime.

FLOW DISTRIBUTION IN THE FILTER CHANNELS

An extra advantage of a one-dimensional model is the information about flow and pressure distribution in the channels, which can be used to give a physical interpretation of the change in trend of the pressure drop for different filters. Knowledge of flow distribution along the channels is crucial for studies of soot and ash accumulation, heat transfer and reaction kinetics.

Combining the pressure drop predictions with the analysis of flow distribution along the axis of the filter can also provide a guidance on the choice of the filter sizes (for example, if a large part of the filter channel is not utilized for filtration, a shorter length filter may be considered). To demonstrate this process, several filter geometries have been analyzed in this section.

Figure 9 shows how the predicted pressure drop for Cores #1, #2 and #4 would change with the filter length and mass flow rate, while keeping all the other parameters constant. Therefore, the filter volume will increase with the length. The length, and thus volume, corresponding to the lowest pressure drop ("optimal length" and "optimal volume" for a fixed diameter), for a given mass flow rate, is marked with a black circle. In a filter with constant diameter, the variation of the length has a double effect on the overall pressure drop. The total loss is the sum of friction and through wall losses, which have opposite trends with respect to the length. The friction losses increase with the increasing of the length, while the through wall losses decrease with the increasing of the length, and vice versa.

The length for which the minimum total loss is achieved is also strongly affected by the permeability, as this changes the contribution of the through wall losses with respect to the friction ones. High values of the permeability decrease the through wall losses (and thus their contribution) and vice versa. This is clearly visible in Figure 9, where for Core #1 (high permeability) the "optimal length" is shorter than for Core #2 and #4 (low permeability). Since coated filters are also used as catalytic converters, this might be beneficial in terms of promoting the chemical reactions, as a bigger volume would increase the residence time. Moreover, for coated filters, the variation of the pressure loss is very small for a large range of filter lengths, which means that from the design point of view there is certain degree of freedom in choosing the filter length.

Figure 10 shows how the predicted pressure drop would change keeping the volume constant ($V = 1.9635 \times 10^5$ $[mm^3]$) and varying the filter length and diameter ("optimal length to diameter ratio" for a fixed volume), which is a common design procedure in sizing the aftertreatment devices. Here it can be seen that the pressure drop increases with the increasing of the length to diameter ratio. However, the coated cores exhibit very little pressure loss change at low length to diameter ratio, which again allows the manufacturers to combine pressure loss considerations with other constraints (i.e. packaging requirements and cost).

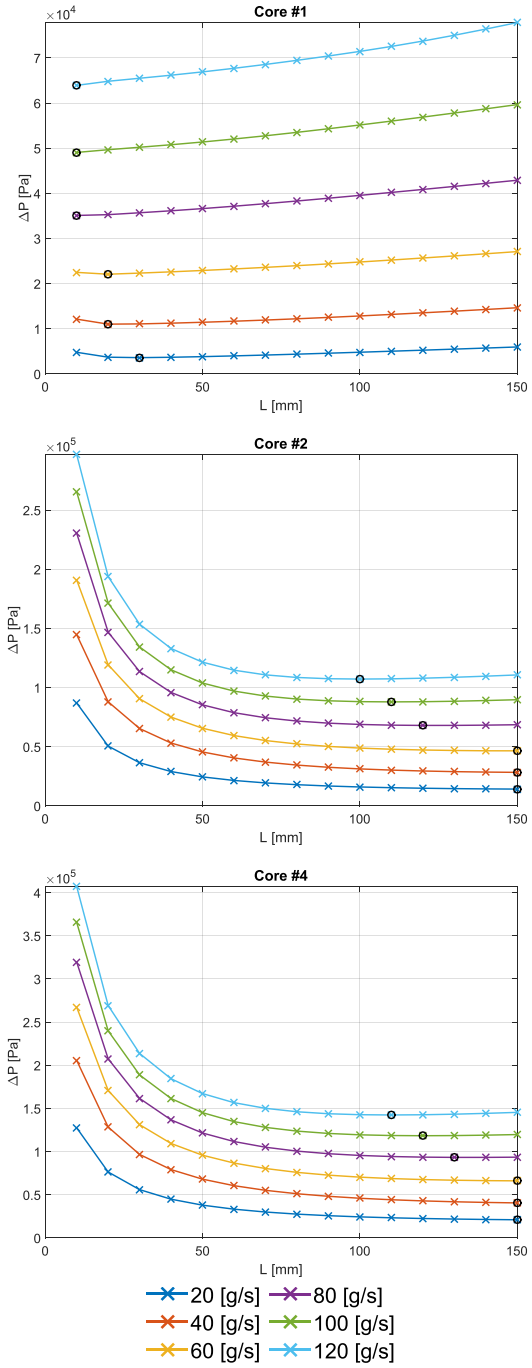

Figure 9. Predicted pressure drop vs filter length with constant filter diameter and different mass flow rate. The black circles indicate the lowest pressure drop for each mass flow rate.

For coated filters, a comparison of Figure 9 and Figure 10 shows that, if the filter diameter is kept constant, increasing the length would be beneficial for reducing pressure loss, while if it is the volume to be kept constant, it would be more beneficial to increase the diameter at the expenses of the length, provided that this does not adversely affect the flow distribution across the filter.

However, the total pressure loss is not the only optimization parameter that needs to be considered. The primary function of the particulate filters is the filtration of the PM and the filtration efficiency is largely affected by other parameters, such as the pore size and the volume of the porous media. Thus, for example, the shorter filters presented in Figure 9 and

Figure 10 would be unpractical for real applications, and they have been plotted here only to illustrate the full trend of the pressure drop and location of the minimum. Additionally, filtration efficiency is linked to the wall flow, and uneven wall flow distribution along the channel axis will affect the soot and ash accumulation patterns.

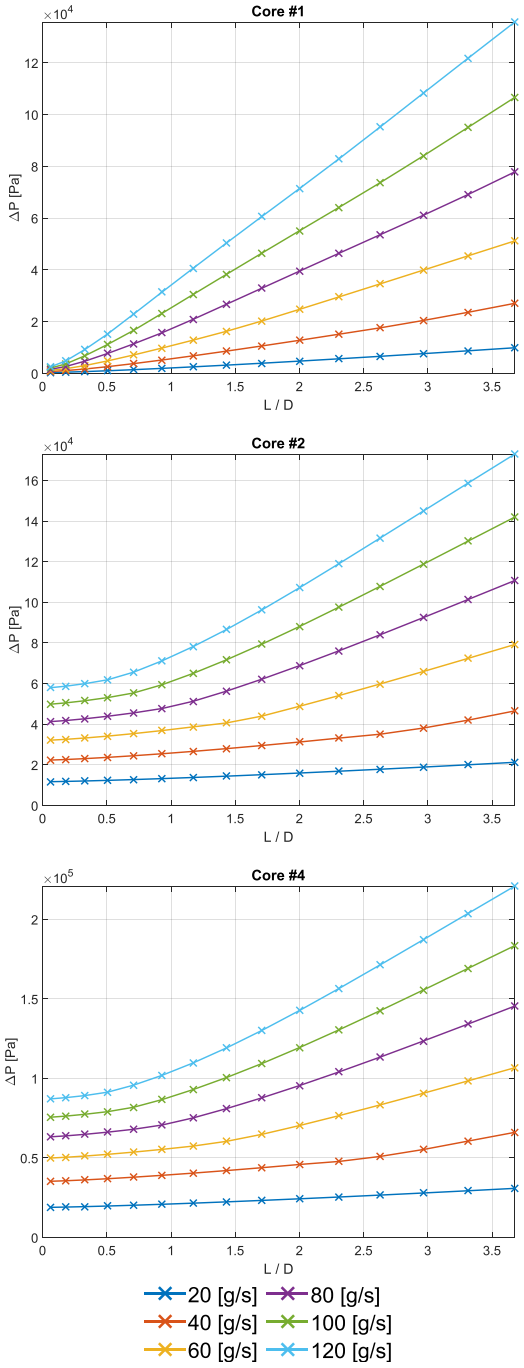

Figure 10. Predicted pressure drop vs filter length to diameter ratio with constant filter volume and different mass flow rate.

Figure 11, Figure 12 and Figure 13 show the predicted dimensional and normalized velocities within the channels and in the porous wall, for three different length $L1 = 50\ [mm]$, $L2 = 100\ [mm]$ and $L3 = 150\ [mm]$, tested at $MFR = 60\ [g/s]$ and $T = 680\ [℃]$ for three filter core specifications.

Figure 11 shows that for the uncoated core the through wall velocities are highly non-uniform, with low values for most of the filter length and a steep increase towards the end. Also, the shortest core shows a slightly less steep velocity increase towards the end, but with a peak of higher magnitude. Instead, for the coated filters, as shown in Figure 12 and Figure 13, the through wall velocities are much more evenly distributed along the channel length and in the shortest filters the velocity is the most uniform.

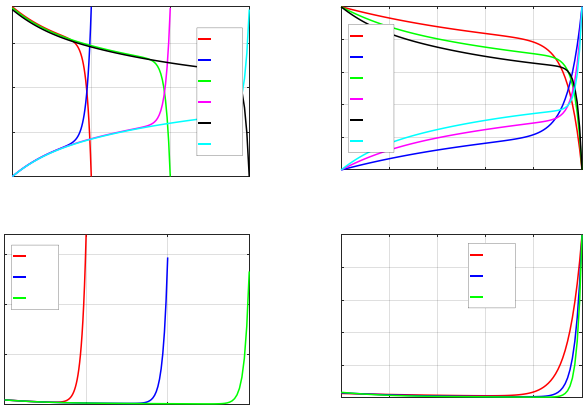

Figure 11. Core #1: Predicted channels and through wall velocities with varying filter length (dimensional values on the left and normalized values on the right).

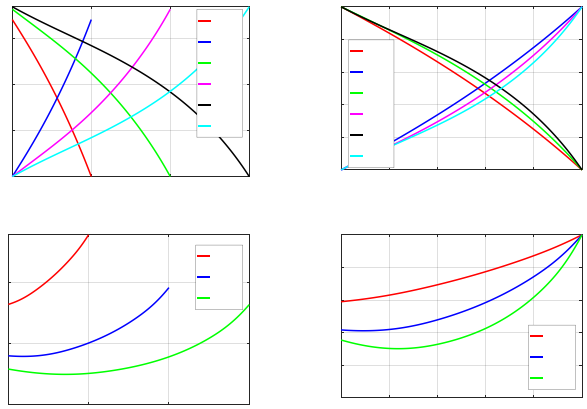

Figure 12. Core #2: Predicted channels and through wall velocities with varying filter length (dimensional values on the left and normalized values on the right).

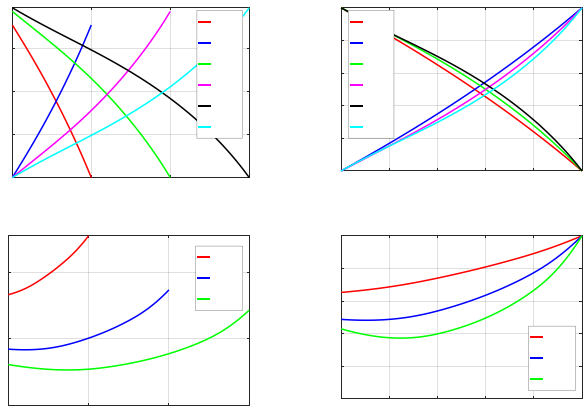

Figure 13. Core #4: Predicted channels and through wall velocities with varying filter length (dimensional values on the left and normalized values on the right).

Although the model indicates that higher wall velocities are expected in the end part of the filter, resulting in more soot accumulated here, the transient nature of soot and ash accumulation means that no definitive conclusions can be made unless the model is modified to account for transient soot layer thickness effects.

Figure 14, Figure 15 and Figure 16 show the predicted dimensional and normalized pressure within the channels for the same test cases.

The pressure difference ($P_1 - P_2$) across the wall reflects the distribution of the through wall velocities, u_w, shown in Figure 11, Figure 12 and Figure 13. For the uncoated filter (Figure 14) the pressure is highly non-uniform in both channels and slowly decreases for most of the filter length; the pressure difference across the wall is small. Towards the end of the filter, the pressures change rapidly producing a relatively large pressure difference and high through wall velocities. In the coated filters (Figure 15 and Figure 16), the pressure is more evenly distributed along the length of the filter, resulting in a more uniform through wall velocity as a consequence of their lower wall permeability. The larger pressure drop for the coated filters means that accounting for the density variation in the model will be more relevant.

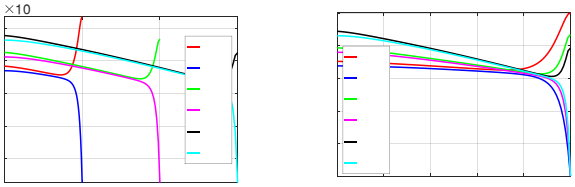

Figure 14. Core #1: Predicted channels pressure with varying filter length (dimensional values on the left and normalized values on the right).

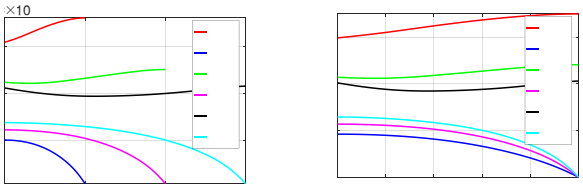

Figure 15. Core #2: Predicted channels pressure with varying filter length (dimensional values on the left and normalized values on the right).

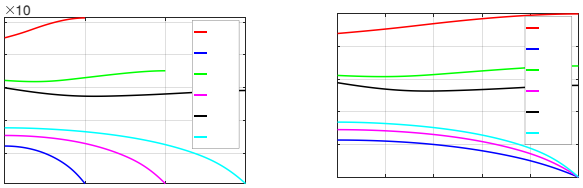

Figure 16. Core #4: Predicted channels pressure with varying filter length (dimensional values on the left and normalized values on the right).

CONCLUSION

A new one-dimensional model has been proposed, which covers both laminar and turbulent flow regimes. The model requires a numerical solution of a one-dimensional boundary value problem, which can be achieved with any available software. Only one parameter (wall permeability) needs to be calibrated from cold flow experimental data in the laminar flow regime, unlike some other laminar flow models that also require inertial loss coefficient calibration.

The model predictions are shown to agree well with experimental data for four different filter cores (with varying cell density, length and permeability), even for very high mass flow rates and temperatures up to $T = 680$ [℃]. The proposed model, thus, effectively extends the Bissett-Kostandopoulos [2] model to the turbulent flow regime and to high temperatures.

The trend of the pressure drop for several parameters and configurations of the filters has been studied as well as the channels' velocity distribution. These studies show how the model could be potentially used as a partial tool (as the pressure drop is not the only relevant parameter) for filter selection or optimization.

A deeper knowledge of the contraction and expansion loss coefficients in the laminar flow regime and the effects that suction/injection and slip flow have on the friction losses may further help in improving the model predictions and strengthen its physical base. Additionally, the effect of the density change can be improved by using the channel local density instead of assuming it as spatially constant. Finally, the model is limited to the prediction of the pressure drop and flow of clean filters. Predictions of loaded filters could be achieved through a deeper understanding of the soot transport and accumulation, and accounting for transient effects. This will be the subject of future work.

REFERENCES

1. Bissett, E.J., "Mathematical Model of the Thermal Regeneration of a wall-flow monolith diesel particulate filter," Chemical Engineering Science 39: 1233-1244, 1984, doi:10.1016/0009-2509(84)85084-8
2. Konstandopoulos, A.G. and Johnson, H., "Wall-Flow Diesel Particulate Filters – Their Pressure Drop and Collection Efficiency," SAE Technical Paper 890405, 1989, doi:10.4271/890405
3. Konstandopoulos, A.G., Skaperdas, E. and Masoudi, M., "Inertial Contributions to the Pressure Drop of Diesel Particulate Filters," SAE Technical Paper 2001-01-0909, 2001, doi:10.4271/2001-01-0909
4. Konstandopoulos, A.G., "Flow Resistance Descriptors for Diesel Particulate Filters: Definitions, Measurements and Testing," SAE Technical Paper 2003-01-0846, 2003, doi:10.4271/2003-01-0846

5. Haralampous, G.A., Kandylas, I. P., Koltsakis, G.S. and Samaras, Z.C., "Diesel Particulate Filter Pressure Drop. Part 1: Modelling and Experimental Validation," International Journal of Engine Research 5(2): 149-162, 2004, doi:10.1243/146808704773564550

6. Masoudi, M., Heible, A. and Then, P.M., "Predicting Pressure Drop of Wall-Flow Diesel Particulate filters - theory and experiment," SAE Technical Paper 2000-01-0184, 2000, doi:10.4271/2000-01-0184

7. Piscaglia, F. and Ferrari, G., "A Novel 1D Approach for the Simulation of Unsteady Reacting Flows in Diesel Exhaust After-Treatment Systems," Energy 34(12): 2051-2062, 2009, doi:10.1016/j.energy.2008.08.022

8. Watling, T.C., Ravenscroft, M.R., Cleeton, J.P.E., Rees, I.D. and Wilkins, D.A.R., "Development of a Particulate Filter Model for the Prediction of Backpressure: Improved Momentum Balance and Entrance and Exit Effect Equations," SAE Int. J. Engines 10(4):1765-1794, 2017, doi:10.4271/2017-01-0974

9. Torregrosa, A.J., Serrano, J.R., Arnau, F.J. and Piqueras, P., "A Fluid Dynamic Model for Unsteady Compressible Flow in Wall-Flow Diesel Particulate Filters," Enegry 36: 671-684, 2011, doi:10.1016/j.energy.2010.09.047

10. Opris, C.N. and Johnson, J.H., "A 2-D Computational Model Describing the Flow and Filtration Characteristics of a Ceramic Diesel Particulate Trap," SAE Technical Paper 980545, 1998, doi:10.4271/980545

11. Oxarango, L., Schmitz, P. and Quintard, M., "Laminar Flow in Channels with Wall Suction or Injection: A New Model to Study Multi-Channels Filtration Systems," Chemical Engineering Science 59: 1039-1051, 2004, doi:10.1016/j.ces.2003.10.027

12. Koltsakis, G., Haralampous, O., Depcik, C. and Ragone, J.C., "Catalyzed Diesel Particulate Filter Modeling," Reviews in Chemical Engineering 29(1): 1-61, 2013, doi:10.1515/revce-2012-0008

13. Yang, S., Deng, C., Gao, Y. and He, Y., "Diesel Particulate Filter Design Simulation: A Review" Adv. Mech. Eng. 8(3): 1-14, 2016, doi:10.1177/1687814016637328

14. Depcik, C., Spickler, B. and Gaire, A., "Revisiting the Single Equation Pressure Drop Model for Perticulate Filters," SAE Technical Paper 2018-01-0952, 2018, doi:10.4271/2018-01-0952

15. Gong, G., Stewart, M.L., Zelenyuk, A., Strzelec, A., Viswanathan, S., Rothamer, D.A., Foster, D.E. and Rutland, C.J., "Importance of Filter's Microstructure in Dynamic Filtration Modelling of Gasoline Particulate Filters (GPFs): Inhomogeneous Porosity and Pore Size Distribution," Chemical Engineering Journal 338: 15-26, 2018, doi:10.1016/j.cej.2018.01.006

16. Korneev, S. and Onori, S., "Transport Model of Particulate in Gasoline Particulate Filter," ASME Proceeding, V002T26A002, 2018, doi:10.1115/DSCC2018-9160

17. Masoudi, M., "Hydrodynamics of Diesel Particulate Filters," SAE Technical Paper 2002-01-1016, 2002, doi:10.4271/2002-01-1016

18. Colebrook, C.F., "Turbulent flow in pipes with particular reference to the transitional region between the smooth and rough pipe laws," Journal of the Institution of Civil Engineers 11(4): 133-156, 1939, doi:10.1680/ijoti.1939.13150

19. Brkić, D., "Review of Explicit Approximations to the Colebrook Relation for Flow Friction," Journal of Petroleum Science and Engineering 77: 34-48, 2011, doi:10.1016/j.petrol.2011.02.006

20. Churchill, S.W., "Friction-factor equation spans all fluid flow regimes," Chemical Engineering 84: 91–102, 1977

21. Jones, O.C., "An Improvement in the Calculation of Turbulent Friction in Rectangular Ducts," Journal of Fluids Engineering 98(2): 173-180, 1976, doi:10.1115/1.3448250

22. Brater, E.F., King, H.W., Lindell, J.E. and Wei, C.Y, "Handbook of Hydraulics, Seventh Edition," (McGraw-Hill, 1996), 6.32-6.37, ISBN 0-07-007247-7

23. Munson, B.R., Young, D.F., Okiishi, T.H., Huebsch, W.W., "Fundamentals of Fluid Mechanics, Sixth Edition," (Wiley, 2009), 415-425, ISBN 978-0470-26284-9

24. Sullivan, J.A., "Fluid Power: Theory and Applications, Third Edition," (Prentice-Hall, 1989), 82, ISBN 0-13-323080-5

25. Merriman, M., "Treatise on Hydraulics, Tenth Edition" (Wiley, 1916), 183

26. Oertel, H., Prandtl, L., Bohle, M., Mayes, K., "Prandtl's Essentials of Fluid Mechanics, Second Edition" (Springer, 2004), 164, ISBN 978-0-387-40437-0

27. Kays, W.M., "Loss Coefficient for Abrupt Changes in Flow Cross Section with Reynolds Number Flow in Single and Multiple Tube Systems," Transactions of the American Society of Mechanical Engineers 72: 1067-1074, 1950

28. Aleksandrova, S., Saul, J., Medina, H., Garcia-Afonso, O., Herreros, J.M., Bevan, M., Benjamin, S.F., "Gasoline Particulate Filter Wall Permeability Testing," SAE Int. J. Engines 11(5):2018, doi:10.4271/03-11-05-0039

DEFINITIONS, ACRONYMS, ABBREVIATIONS

DPF	Diesel Particulate Filter
GPF	Gasoline Particulate Filter
MFR	Mass Flow Rate
OFA	Open Frontal Area

PM	Particulate Matter
VFM	Viscous Flow Meter

NOMENCLATURE

A_1	$[m^2]$	Cross-sectional area of the smaller channel
A_2	$[m^2]$	Cross-sectional area of the larger channel
c	$[-]$	Constant for Eq. (27)
C_1	$[-]$	Arbitrary constant for laminar flow trend
C_2	$[-]$	Arbitrary constant for turbulent flow trend
C_f	$[-]$	Fanning friction factor
$C_{f,i}$	$[-]$	Local Fanning friction factor
D	$[m]$	Filter diameter
d_h	$[m]$	Cell hydraulic diameter
k	$[m^2]$	Filter permeability
L	$[m]$	Filter length
M	$[kg/mol]$	Molar mass
$P_{Atm.}$	$[Pa]$	Atmospheric pressure
P_i	$[Pa]$	Local mean pressure in the channel
P^*	$[-]$	Dimensionless pressure
R	$\left[\frac{kg\ m^2}{mol\ ℃\ s^2}\right]$	Gas constant
Re	$[-]$	Reynolds number at the entrance of the inlet channel
Re_i	$[-]$	Local channel Reynolds number
$Re_{Circular,i}$	$[-]$	Local channel Reynolds number for ducts of circular cross-section
$Re_{Square,i}$	$[-]$	Local channel Reynolds number for ducts of square cross-section
T	[℃]	Temperature
$U = \frac{MFR}{\rho\ OFA}$	$[m/s]$	Mean velocity at the entrance to the filter inlet channel
u_i	$[m/s]$	Local mean cross-sectional axial velocity along the channel
u_w	$[m/s]$	Local mean cross-sectional velocity along the porous wall
V	$[m^3]$	Volume
w_s	$[m]$	Porous wall thickness
x	$[m]$	Axial coordinate

GREEK LETTERS

ε	$[-]$	Surface roughness
$\zeta_{Contr.}$	$[-]$	Contraction loss coefficient
$\zeta_{Exp.}$	$[-]$	Expansion loss coefficient
μ	$[kg/(m\ s)]$	Dynamic viscosity
ρ	$[kg/m^3]$	Density
ρ_{Inlet}	$[kg/m^3]$	Density at the entrance of the inlet channel
ρ_{Outlet}	$[kg/m^3]$	Density at the exit of the outlet channel

SUBSCRIPT

i	Index referring either to inlet (1) or outlet (2) cell
it	Iteration